

## Analysis of Figure-8-Undulator Radiation

Takashi Tanaka<sup>a</sup> and Hideo Kitamura<sup>b</sup>

<sup>a</sup>Department of Nuclear Engineering, Kyoto University, Yoshida-Honmachi, Sakyo-ku, Kyoto 606-01, Japan, and <sup>b</sup>JAERI-RIKEN SPring-8 Project Team, SPring-8, Kamigori-cho, Hyogo 678-12, Japan

(Received 23 October 1995; accepted 2 January 1996)

The figure-8 undulator is a novel insertion device which has recently been proposed in order to obtain linearly polarized radiation with low on-axis power density. Since the trajectory is different from any other insertion device developed or proposed so far, the features of figure-8-undulator radiation are also considered to be different. In this paper, various features of figure-8-undulator radiation are investigated to clarify differences between the figure-8 undulator and other ordinary insertion devices.

**Keywords:** figure-8 undulator; spatial distribution; polarization; power density.

### 1. Introduction

Although many kinds of insertion devices have been developed or proposed since the start of the utilization of synchrotron radiation, such devices are classified into two types. One is the planar type whose electron trajectory lies in a plane, and the other is the helical or elliptical type whose electron trajectory rotates along the beam axis.

In the previous paper (Tanaka & Kitamura, 1995), we proposed a new type of insertion device, called a figure-8 undulator, for linearly polarized radiation. It has the advantage that the on-axis power density is much lower than that of an ordinary planar undulator when high  $K$  values are applied. The trajectory of the figure-8 undulator has an eight-figured shape when projected on the transverse plane, which differs from those of any other insertion devices that have been developed or proposed so far. Therefore, the features of figure-8-undulator radiation are considered to be different from those of ordinary insertion devices.

In this paper, analysis of figure-8-undulator radiation is made in order to clarify the difference between the figure-8 undulator and other insertion devices, for the practical use of the figure-8 undulator as a third-generation synchrotron source.

### 2. Equations on figure-8-undulator radiation

A schematic illustration of the figure-8 undulator is shown in Fig. 1. Although it is similar to the helical undulator (Kimura *et al.*, 1995), the period length of the magnet array generating the vertical field (horizontal undulator) is twice as long as that generating the horizontal field (vertical undulator). The magnetic field in the figure-8 undulator is given by the equations

$$B_x = -B_{x0} \sin(\pi z/\lambda_u), \quad (1)$$

$$B_y = B_{y0} \sin(2\pi z/\lambda_u), \quad (2)$$

where  $\lambda_u$  is the period length of the horizontal undulator and  $B_{x0}$  and  $B_{y0}$  are the peak magnetic fields. Solving the equations of motion we obtain the position and relative velocity as

$$r(t) = c\beta \left\{ \begin{aligned} &\frac{K_y}{\omega_0\gamma} \sin(\omega_0 t), \quad \frac{2K_x}{\omega_0\gamma} \sin(\omega_0 t/2), \\ &\left[ \left( 1 - \frac{K_x^2 + K_y^2}{4\gamma^2} \right) t - \frac{K_x^2}{4\omega_0\gamma^2} \sin(\omega_0 t) \right. \\ &\quad \left. - \frac{K_y^2}{8\omega_0\gamma^2} \sin(2\omega_0 t) \right] \end{aligned} \right\}, \quad (3)$$

$$\beta(t) = \beta \left[ \begin{aligned} &\frac{K_y}{\gamma} \cos(\omega_0 t), \quad \frac{K_x}{\gamma} \cos(\omega_0 t/2), \\ &1 - \frac{(K_x^2 + K_y^2)}{4\gamma^2} - \frac{K_x^2}{4\gamma^2} \cos(\omega_0 t) \\ &\quad - \frac{K_y^2}{4\gamma^2} \cos(2\omega_0 t) \end{aligned} \right] \quad (4)$$

where

$$\omega_0 = (2\pi\beta c/\lambda_u)[1 - (K_x^2 + K_y^2)/4\gamma^2], \quad (5)$$

$$K_x = (eB_{x0}\lambda_u)/(\pi mc), \quad (6)$$

$$K_y = (eB_{y0}\lambda_u)/(2\pi mc). \quad (7)$$

The electric field of radiation generated by an electron moving along an arbitrary trajectory is given by

$$\mathbf{E} = \frac{e}{4\pi\epsilon_0 cR} \left[ \frac{\mathbf{n} \times \{(\mathbf{n} - \beta \times \dot{\beta})\}}{(1 - \mathbf{n} \cdot \beta)^3} \right]_t, \quad (8)$$

where  $\mathbf{n}$  is a unit vector directed from  $\mathbf{r}$  to the observer,  $R$  is the distance between  $r$  and the observer, and  $t'$  is the retarded time. The Fourier transformation of  $\mathbf{E}$  is calculated as

$$\mathbf{E}_\omega = \sum_{k=1}^{\infty} \mathbf{E}_k, \quad (9)$$

$$\mathbf{E}_k = \frac{iek(\omega_1/2)^2 N}{8\pi^2 \epsilon_0 c R} \exp[-i(\omega_1/2)kR/c] \times \mathbf{n} \times (\mathbf{n} \times \mathbf{Q}_k) P_N \quad (10)$$

where

$$\omega_1 = \frac{4\pi c \gamma^2 / \lambda_u}{1 + (K_x^2 + K_y^2)/2 + \gamma^2 \theta^2}, \quad (11)$$

$$P_N = \frac{\sin[\pi N(k/2 - \omega/\omega_1)]}{\pi N(k/2 - \omega/\omega_1)}, \quad (12)$$

$$\mathbf{Q}_k = \int_0^{4\pi/\omega_1} \beta(\mathbf{t}) \exp[-i\omega_1(k/2)(t - \mathbf{n} \cdot \mathbf{r}(t)/c)] dt. \quad (13)$$

Substituting (3) and (4), the  $x$  component of  $\mathbf{Q}_k$  is calculated as

$$Q_{kx} = \frac{2K_y}{\gamma\omega_0} \int_0^{2\pi} \cos 2\eta \exp\{i[k\eta - X \sin \eta + Y \sin(2\eta) + Z \sin(4\eta)]\} d\eta, \quad (14)$$

where

$$X = 4\xi K_x \gamma \theta \sin \phi, \quad (15)$$

$$Y = \xi [(K_x^2/2) - 2K_y \gamma \theta \cos \phi], \quad (16)$$

$$Z = \xi K_y^2/4. \quad (17)$$

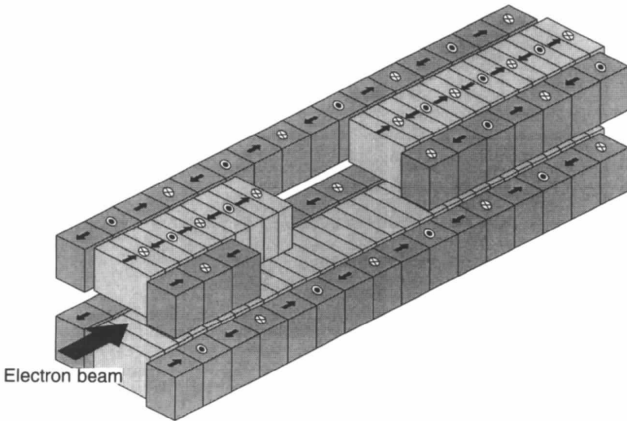


**Figure 1** Schematic illustration of the figure-8 undulator. The period length of the vertical undulator is twice as long as that of the horizontal undulator.

$$\xi = (k/2)/[1 + (K_x^2 + K_y^2)/2 + \gamma^2 \theta^2]. \quad (18)$$

Using the relation

$$\exp[i(x \sin y)] = \sum_{p=-\infty}^{\infty} J_p(x) \exp(ip y), \quad (19)$$

equation (14) is rewritten as

$$Q_{kx} = \frac{2\pi K_y}{\gamma\omega_0} \sum_p \sum_q [J_{k+2q+4p+2}(X) + J_{k+2q+4p-2}(X)] J_q(Y) J_p(Z). \quad (20)$$

In a similar manner, we obtain

$$Q_{ky} = \frac{2\pi K_x}{\gamma\omega_0} \sum_p \sum_q [J_{k+2q+4p+1}(X) + J_{k+2q+4p-1}(X)] J_q(Y) J_p(Z), \quad (21)$$

$$Q_{kz} = \frac{4\pi}{\omega_0} \sum_p \sum_q J_{k+2q+4p}(X) J_q(Y) J_p(Z). \quad (22)$$

Decomposing  $\mathbf{E}_k$  into two polarization components, we obtain

$$E_{k\parallel}(\omega) = \frac{ie\omega_1 \gamma \exp(-i\omega_1 kR/c)}{2\epsilon_0 c R} f_x(\gamma\theta, \phi), \quad (23)$$

$$E_{k\perp}(\omega) = \frac{ie\omega_1 \gamma \exp[-i\omega_1 kR/c]}{2\epsilon_0 c R} f_y(\gamma\theta, \phi), \quad (24)$$

where

$$f_x(\gamma\theta, \phi) = \xi [2S_0 \gamma \theta \cos \phi - K_y (S_2 + S_{-2})] P_N, \quad (25)$$

$$f_y(\gamma\theta, \phi) = \xi [2S_0 \gamma \theta \sin \phi - K_x (S_1 + S_{-1})] P_N, \quad (26)$$

$$S_j = \sum_{p=-\infty}^{\infty} \sum_{q=-\infty}^{\infty} J_{2n+2q+4p+j}(X) J_p(Y) J_q(Z). \quad (27)$$

$E_{k\parallel}$  and  $E_{k\perp}$  represent the components parallel and vertical to the horizontal plane, respectively. It is found from the above equations that the polarization is linear for each harmonic since both components have the same phase.

From (12), it is found that the peak energy of the  $k$ th harmonic is  $k\omega_1/2$ . In order to take  $\omega_1$  to be the energy of the fundamental radiation, we introduce a new harmonic number,  $n$ , defined as

$$n = k/2. \quad (28)$$

Finally, the photon flux density of the  $n$ th harmonic is calculated as

$$\frac{d^2 P_n}{d\Omega d\omega} = \frac{e^2 \gamma^2 N^2}{4\pi \epsilon_0} (f_x^2 + f_y^2). \quad (29)$$

### 3. Analysis

Now let us analyse the features of figure-8-undulator radiation. For example, the value  $(K_x^2 + K_y^2)^{1/2}$  is assumed to be 4.72, the ratio  $K_x/K_y$  unity (figure-8 and helical undulators) or zero (planar undulator), the period length 10 cm, the number of periods 44, the electron energy 8 GeV and the average current 100 mA. In this case, the energy of the fundamental is 500 eV.

#### 3.1. Polarization

Figs. 2(a) and 2(b) show the spatial dependence of the direction and the amplitude for the fundamental radiation

obtained from the planar and figure-8 undulators, respectively. In these figures, the length and direction of each bar show the amplitude normalized by the on-axis value and the direction of polarization, respectively.

In the case of the planar undulator, the radiation is polarized almost in the horizontal plane for values of  $\gamma\theta$  smaller than 1.0, while for larger values the plane of polarization rotates along the contour. In the case of the figure-8 undulator, the rotation of the plane of polarization along the contour is more prominent than in the previous case, which means that the degradation of the degree of polarization due to the angular divergence of the beam and the size of the slit is also more prominent.

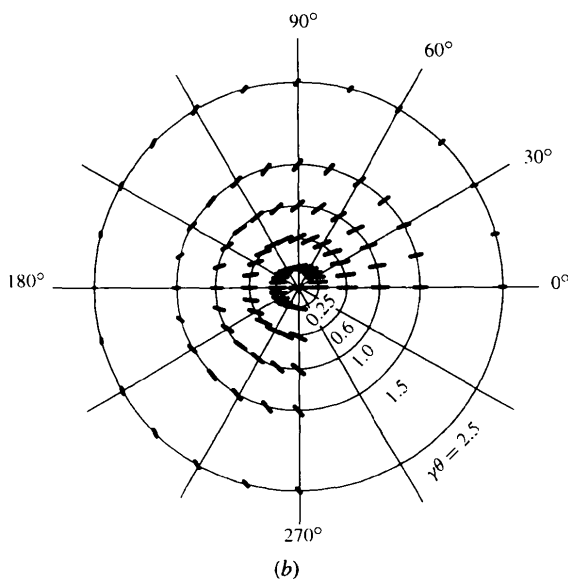
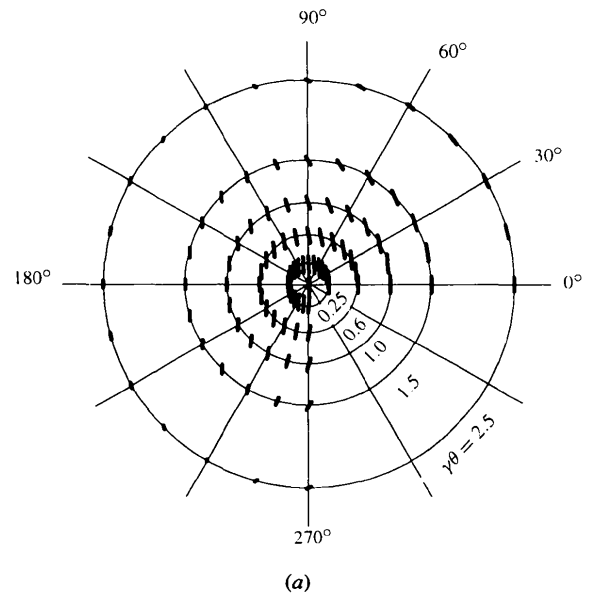
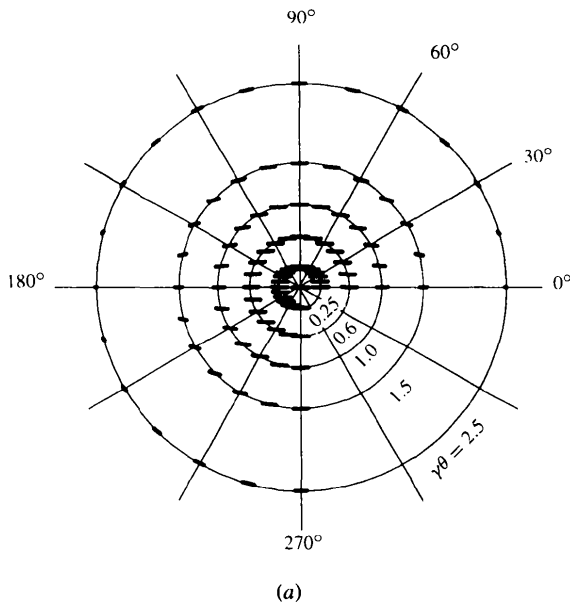


**Figure 2**  
Spatial distribution of the amplitude and the direction of polarization for the fundamental radiation in the case of (a) the planar undulator, and (b) the figure-8 undulator.

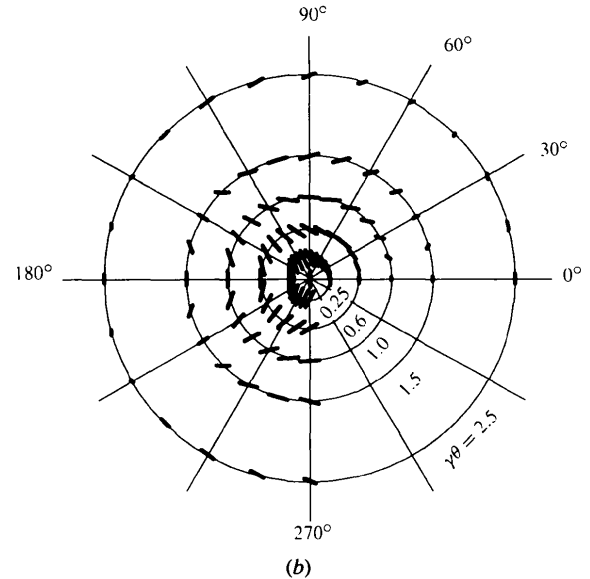


**Figure 3**  
Spatial distribution of the amplitude and the direction of polarization for (a) the 0.5th harmonic, and (b) the 1.5th harmonic, in the case of the figure-8 undulator.

The direction/amplitude of the figure-8 undulator are asymmetric/symmetric with respect to the vertical observation angle,  $\theta_y(\theta \sin \phi)$ , while they are asymmetric with respect to the horizontal observation angle,  $\theta_x(\theta \cos \phi)$ . This is similar to the case of the spatial distribution of the power density. They are derived from the asymmetry of  $\beta_y$  with respect to  $\beta_x$ .

The slope of the direction of polarization is equal to zero both along  $\theta_x$  and  $\theta_y$  in the case of the planar undulator. On the other hand, that of the figure-8 undulator increases along the  $\theta_y$  axis, which means that the degree of polarization degrades. Therefore, the coupling constant of the storage ring and the vertical size of the slit should be as small as possible in order to obtain a high degree of polarization.

Figs. 3(a) and 3(b) show the spatial dependence of the direction and the amplitude for the 0.5th and the 1.5th

harmonics obtained from the figure-8 undulator. As well as the fundamental, the direction and the amplitude are asymmetric with respect to  $\theta_x$  for both harmonics. For the 0.5th harmonic, the radiation is polarized in the vertical plane when observed on-axis, and the rotation of the plane of polarization for larger values of  $\gamma\theta$  is not as prominent as that for the fundamental, which may result in a high degree of polarization even when the size of the slit and the divergence of the beam is large. For the 1.5th harmonic, the polarization on-axis is vertical, as is that of the 0.5th harmonic. However, the rotation of the plane of polarization is more notable. Therefore, the degree of polarization may degrade more rapidly than that of the 0.5th harmonic.

3.2. Spatial distribution of radiation

Integrating (29) over  $\omega$ , we obtain the partial power density for the  $n$ th harmonic. If this value is large for higher harmonics, it is expected that the power density will be

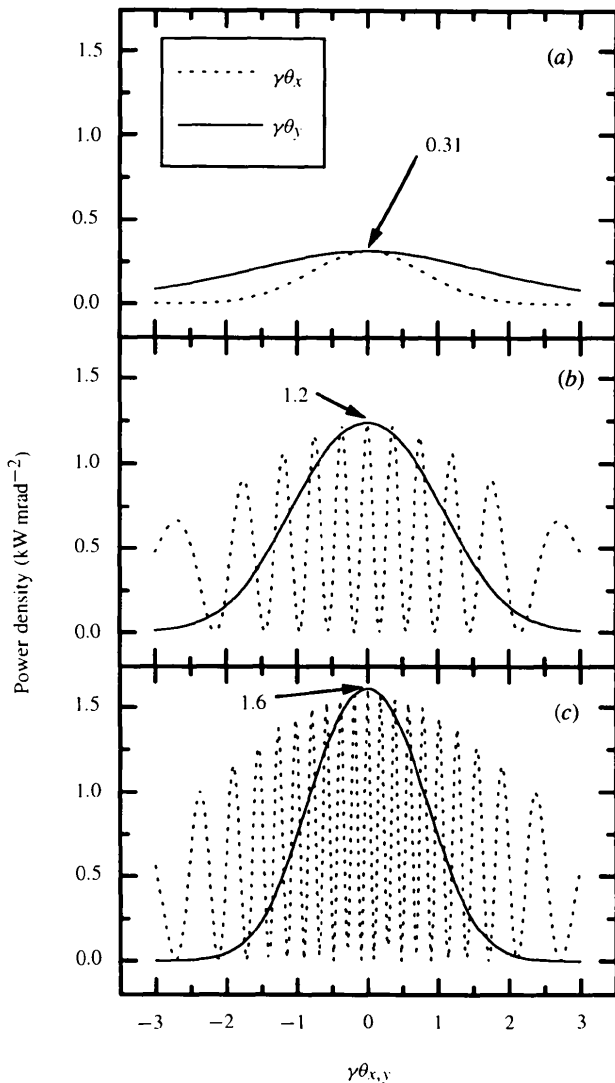


**Figure 4**  
Angular distribution of the partial power density for (a) the fundamental, (b) the 11th harmonic, and (c) the 21st harmonic in the case of the planar undulator. The solid curve shows the distribution along  $\theta_y$  and the dashed curve the distribution along  $\theta_x$ .

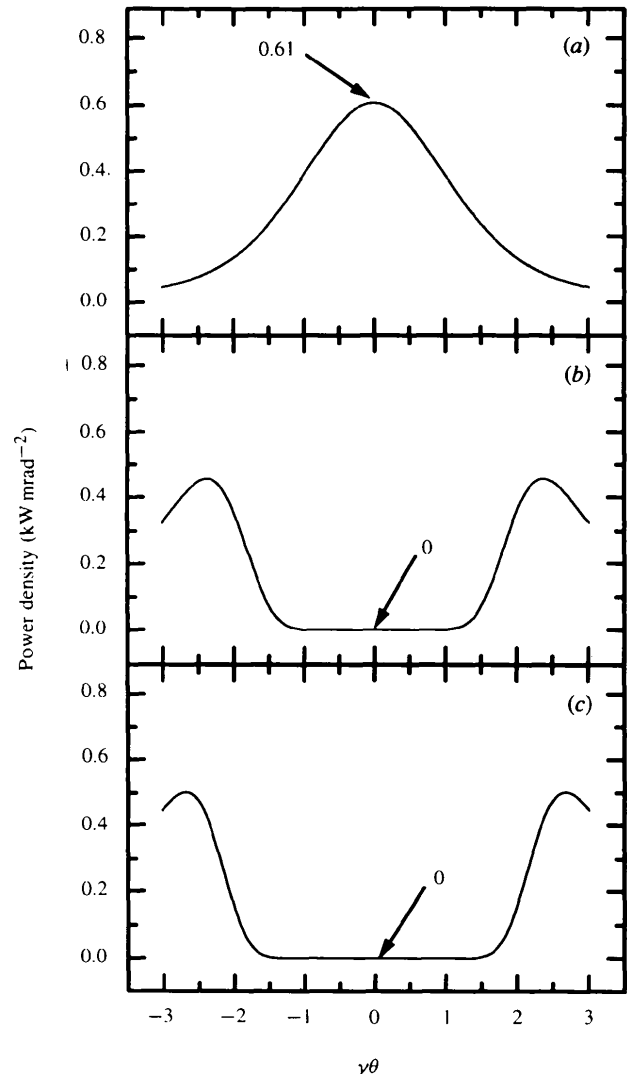


**Figure 5**  
Same as Fig. 4 but in the case of the figure-8 undulator.

unreasonably high due to the contribution of the unwanted higher harmonics.

Figs. 4(a)–4(c) show the partial power density as a function of  $\theta_x(\theta \cos \phi)$  and  $\theta_y(\theta \sin \phi)$  for various harmonics in the case of the planar undulator. From these figures, it is found that the radiated power derived from higher harmonics distributes on-axis as well as for the fundamental. The total power density on-axis is calculated as  $98 \text{ kW mrad}^{-2}$ . Therefore, the ratio of the partial power density for the fundamental to the total is  $3.16 \times 10^{-3}$ , which is extremely low.

Figs. 5(a)–5(c) correspond to Figs. 4(a)–4(c) in the case of the figure-8 undulator. From these figures, it is found that the power for higher harmonics distributes mainly off-axis, while that for the fundamental distributes on-axis. Therefore, one can use the fundamental radiation without being concerned by the unreasonable heat load brought by the higher harmonics. The total power density is calculated

as  $1.4 \text{ kW mrad}^{-2}$ . Therefore, the ratio of the partial power density for the fundamental to the total is 0.16, which is sufficiently high.

Figs. 6(a)–6(c) show the partial power density of the helical undulator as a function of  $\theta$ . Since the distribution is uniform with respect to  $\phi$ , we set  $\phi = 0$ . Since no higher harmonics are observed on-axis, the power density of higher harmonics is equal to zero and the on-axis total power density is equal to the on-axis partial power density of the fundamental. As well as the figure-8 undulator, the power density for higher harmonics is a maximum at  $\gamma\theta = 2.5$ . The on-axis partial power density for the fundamental is larger than that of the other two undulators.

Figs. 7(a)–7(c) show examples of the spectra of the figure-8 undulator at various angles of observation. In each figure the vertical angle,  $\theta_y$ , is set to zero. It is clear that at  $\theta = -2.5/\gamma$  the contribution of the higher harmonics to the

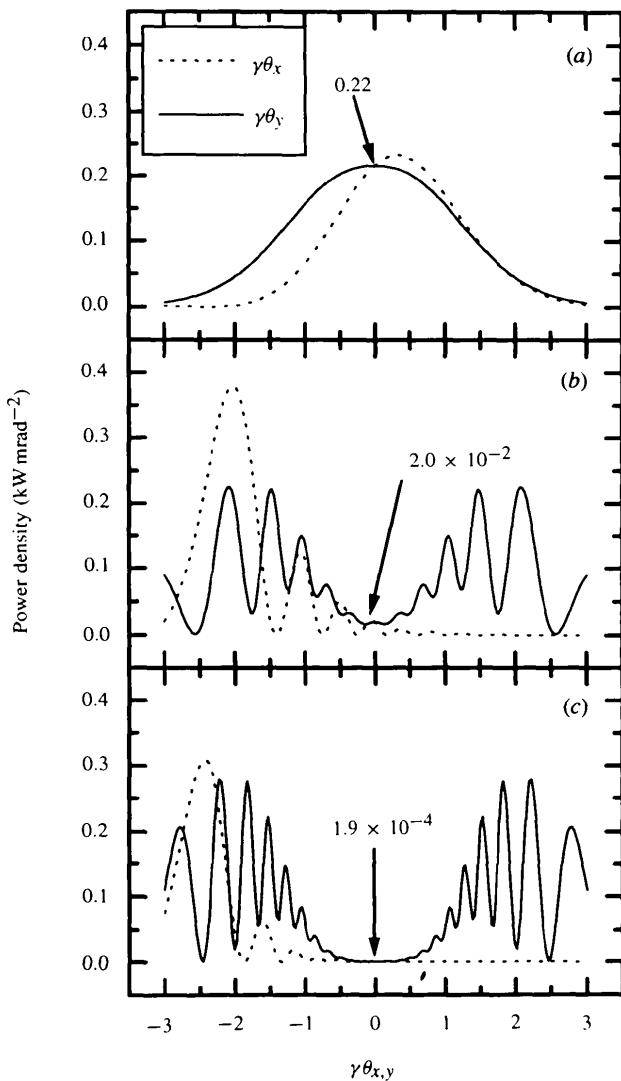


**Figure 6**  
Same as Fig. 4 but in the case of the helical undulator. Only the distribution along  $\theta$  is shown because of the uniformity with respect to  $\phi$ .

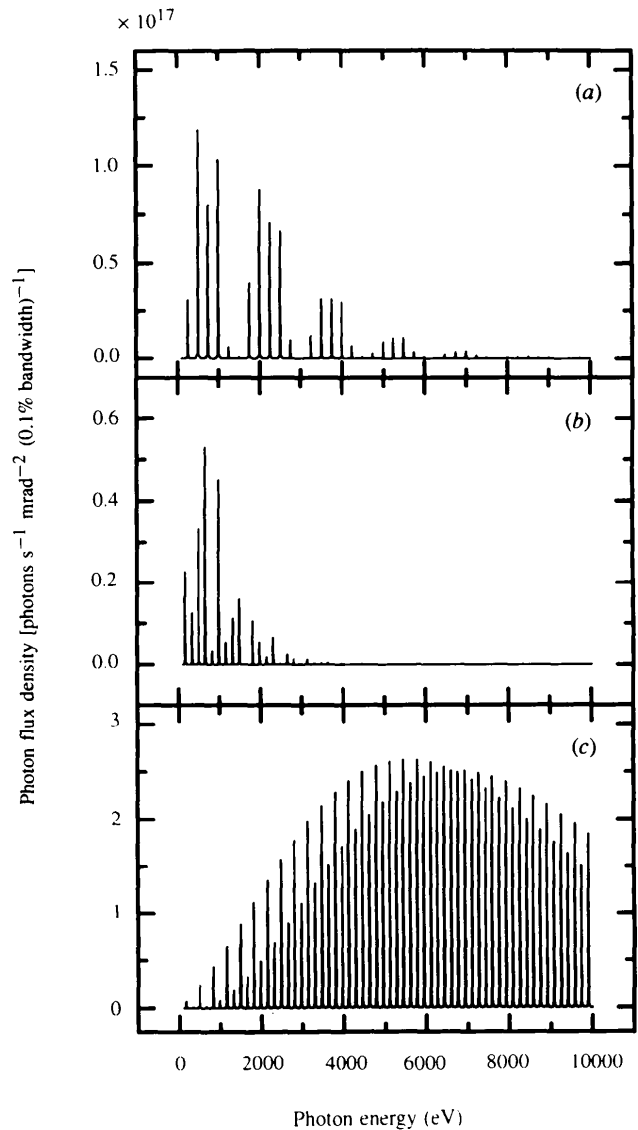


**Figure 7**  
Spectra of the figure-8 undulator observed (a) on-axis, (b) at  $\theta_x = 2.5/\gamma$ , and (c) at  $\theta_x = -2.5/\gamma$ .  $\theta_y$  is set to zero in each case.

spectrum is much larger than in the other two cases, which is expected from Figs. 5(a)–5(c).

#### 4. Summary

We have investigated various features of figure-8-undulator radiation. The results are summarized below:

- (i) In order to achieve a high degree of polarization, the vertical size of the aperture should be as small as possible;
- (ii) Reasonable utilization of the fundamental radiation is possible with little heat load brought by unwanted

higher harmonics because the radiated power of the higher harmonics exists off-axis. This is similar to the case of the helical undulator.

#### References

- Kimura, S., Kamada, M., Hama, H., Maréchal, X. M., Tanaka, T. & Kitamura, H. (1995). *Proc. Int. Conf. VUV '95 (VUV11)*. To be published.
- Tanaka, T. & Kitamura, H. (1995). *Nucl. Instrum. Methods*, **A364**, 368–373.